Characterization of highly-oriented ferroelectric $Pb_xBa_{1-x}TiO_3$ thin films grown by metalorganic chemical vapor deposition

Mohamed Y. El-Naggar, David A. Boyd, and David G. Goodwin[a)]
Division of Engineering and Applied Science, California Institute of Technology, Pasadena, California 91125

(Received 2 May 2005; accepted 28 June 2005)

$Pb_xBa_{1-x}TiO_3$ ($0.2 \leqslant x \leqslant 1$) thin films were deposited on single-crystal MgO as well as amorphous Si_3N_4/Si substrates using biaxially textured MgO buffer templates, grown by ion beam-assisted deposition (IBAD). The ferroelectric films were stoichiometric and highly oriented, with only (001) and (100) orientations evident in x-ray diffraction (XRD) scans. Films on biaxially textured templates had smaller grains (60 nm average) than those deposited on single-crystal MgO (300 nm average). Electron backscatter diffraction (EBSD) has been used to study the microtexture on both types of substrates and the results were consistent with x-ray pole figures and transmission electron microscopy (TEM) micrographs that indicated the presence of 90° domain boundaries, twins, in films deposited on single-crystal MgO substrates. In contrast, films on biaxially textured substrates consisted of small single-domain grains that were either *c* or *a* oriented. The surface-sensitive EBSD technique was used to measure the tetragonal tilt angle as well as in-plane and out-of-plane texture. High-temperature x-ray diffraction (HTXRD) of films with 90° domain walls indicated large changes, as much as 60%, in the *c* and *a* domain fractions with temperature, while such changes were not observed for $Pb_xBa_{1-x}TiO_3$ (PBT) films on biaxially textured $MgO/Si_3N_4/Si$ substrates, which lacked 90° domain boundaries.

I. INTRODUCTION

High-frequency response and work output per unit volume are two important figures of merit for microactuator materials.[1] Taking this into account, ferroelectrics are candidate materials since actuation can be achieved by directly applying electric fields. As a ferroelectric, the solid solution system $Pb_xBa_{1-x}TiO_3$ (PBT) is [001] polarized at room temperature (tetragonal) and is cubic above the Curie temperature, T_c. The polarization direction may lie along any of the six equivalent ⟨100⟩ directions, and this direction of polarization can be switched by applied electric fields or mechanical loads. The switching is accompanied by a reorientation of the tetragonal unit cell and can lead to a strain corresponding to $c/a - 1$, where c/a is the ratio of lattice parameters. In principle, this strain is about 1% for $BaTiO_3$ (BT) and 6.3% for $PbTiO_3$ (PT).[2] Furthermore, the mobility of 90° domain walls is expected to be a function of composition as the Curie temperature varies monotonically with composition, from 120 °C for BT to 490 °C for PT. The ability to tune the composition of the ferroelectric thin film, and consequently the strain and response time, may allow flexibility in material design.

To achieve the high strains associated with the *c/a* ratio, PBT must be utilized in single-crystal or highly textured thin film forms in order to be completely cycled between two different polarized states.[3,4] Metalorganic chemical vapor deposition (MOCVD) has been shown to be an excellent technique for depositing PT on various substrates,[5–10] including on MgO.[11–13] BT has also been successfully deposited on MgO using metalorganic chemical vapor deposition (MOCVD).[14,15] Despite this, little work has been done on MOCVD of the PBT system. Results available in the literature for MOCVD PBT on Pt/Si[16] indicated ferroelectric behavior only for $x > 0.8$ and strongly distorted *c/a* ratios (<1 for $x < 0.8$) where the distortions were attributed to film stress.

In this study, we report the successful deposition of highly oriented, ferroelectric PBT ($0.2 \leqslant x \leqslant 1$) thin films on both commercially obtained single-crystal MgO (used as received) substrates as well as amorphous Si_3N_4/Si using 20-nm IBAD (ion beam-assisted deposition) MgO followed by 20-nm homoepitaxial MgO, as a templating layer. Details on the IBAD MgO process can be found in reference #17. MgO is used as a substrate because the lattice parameter (4.213 Å) is reasonably well matched to the lattice parameters of tetragonal BT

a)Address all correspondence to this author.
e-mail: dgoodwin@caltech.edu
DOI: 10.1557/JMR.2005.0374

(c = 4.038 Å, a = 3.994 Å) and PT (c = 4.151 Å, a = 3.905 Å). Furthermore, it has been demonstrated[17,18] that IBAD MgO on amorphous Si_3N_4 develops a narrow biaxial texture and is therefore suitable as a buffer layer to integrate PBT with Si-based substrates.

A detailed characterization of the microstructure is presented using a variety of techniques, for PBT on both types of substrates. There is evidence that the ferroelectric and fatigue properties of thin films depend on crystallite orientation.[19–21] Detailed texture analysis is, consequently, a crucial method in the characterization of ferroelectric-based electronic and MEMS devices. We use electron backscatter diffraction (EBSD) to confirm the presence of 90° domain walls and to study the crystallographic texture in PBT thin films, in addition to x-ray pole figures.

II. EXPERIMENTAL

The MOCVD reactor used in this study is a custom-built, warm-wall stagnation-flow reactor with a vertical showerhead.[22] The reactor features a precursor delivery system that allows for closed-loop control of gas-phase stoichiometry during deposition to produce PBT films of varying compositions. The Ba, Pb, and Ti precursors are $Ba(C_{11}H_{19}O_2)_2$, $Pb(C_{11}H_{19}O_2)_2$, and $Ti[OCH(CH_3)_2]_2[C_{11}H_{19}O_2]_2$, respectively. The precursors are kept in bubblers inside separate ovens to sublimate at their specific temperatures. Table I lists typical experimental settings for the precursors and growth conditions.

The stoichiometry control is accomplished using an ultraviolet-based control loop. Ultraviolet (UV)-based precursor control has been demonstrated in the literature for YBCO superconducting thin films.[22,23] The precursors have distinct absorption features in the ultraviolet spectrum. These features have been characterized and appropriate wavelengths chosen for control purposes. The control wavelengths chosen were 290, 300, and 330 nm for the Ba, Pb, and Ti precursors, respectively. The solid precursors sublimate in the temperature controlled bubblers under the reduced pressure and are then passed through separate optical cells, kept at 250 °C. At each cell, the UV signal strength indicates the concentration of the specific precursor. Active control in the feedback loop is accomplished by changing the carrier gas flow rate (3 SLM Ar total) through the individual bubblers. The total precursor flow rate is typically kept at 75 μmol/min. The precursors are then combined and subsequently mixed with 2 SLM O_2 and passed through a showerhead onto the heated substrate in the vertical stagnation-flow reactor. A typical growth rate resulting from this procedure is 3–4 nm/min of PBT.

TABLE I. Typical growth conditions for MOCVD of PBT films on MgO.

Pb precursor temperature	135 °C
Ba precursor temperature	236 °C
Ti precursor temperature	130 °C
Total carrier gas flow rate	3 SLM
O_2 flow rate	2 SLM
Reactor pressure	15 Torr
Substrate temperature	650 °C

The microstructure, surface morphology, and chemical composition of the PBT thin films were studied using a scanning electron microscope (LEO 1550 VP field emission SEM) equipped with an energy-dispersive spectrometer (EDS). Quantitative analyses of stoichiometry were performed using an electron micro-probe analyzer (Jeol JXA-733 EMPA) with sampling volumes of a few cubic microns, corresponding to a weight of a few picograms.

The crystallinity and phase purity were examined using θ–2θ XRD scans (Philips X'Pert PRO MPD diffractometer) indicating the orientation of the deposited thin films, while scans conducted at higher temperatures were used to investigate domain switching and produced quantitative information regarding the abundance of specific domains in the films. Scans were typically collected from 2θ = 10° to 2θ = 80°.

Detailed domain characterization was accomplished by pole figure techniques (Philips X'Pert equipped with a texture cradle) and the results were compared to electron backscatter diffraction (EBSD) data. In recent years, EBSD has emerged as a powerful characterization tool for probing the microtexture of materials. The combination of high surface sensitivity, high spatial resolution (~50 nm in a field emission SEM), and large spatial extent (using computer controlled stages) cannot be matched using traditional texture techniques.[24] In this study, we applied EBSD to study the texture of the ferroelectric thin films. Only samples with high Pb content ($x \geqslant 0.8$) were analyzed using this technique, as the increased tetragonal distortion makes it easier to distinguish between c and a domains during the automated indexing. The domain fractions and tetragonal tilt angles measured by EBSD, specifically on Pb-rich films with $c/a \geqslant 1.05$, produced results consistent with x-ray pole figure analysis. The tilt angle between c and a domains, δ, accompanying the tetragonal distortion is especially useful for detecting domain boundaries. For $c/a \geqslant 1.05$, $\delta \geqslant 2.8°$ while the minimum measurable dispersion in orientation, using EBSD, is 1°.[24] Square regions of a few microns on each side were typically analyzed using grid points 50 nm apart for a total of a few thousand patterns from each sample.

III. RESULTS AND DISCUSSION

A. Orientation

Only (*h*00) and (00*l*) PBT peaks were observed in θ–2θ XRD spectra, indicating that the *c* and *a* axes of the tetragonal phase are either in or out of the plane of the substrate exclusively. Figure 1 compares the θ–2θ spectra of two PBT films ($x = 0.8$, 0.5 μm thick). The film grown on single-crystal MgO is predominantly *c*-axis (out-of-plane)-oriented, while PBT on the biaxially textured $MgO/Si_3N_4/Si$ substrate is mostly *a*-axis-oriented. The difference is attributed to the low thermal expansion coefficient of the Si substrate compared to MgO single crystal substrates ($\alpha_{Si} = 2.6 \times 10^{-6}$/K,[25] $\alpha_{MgO} = 14.8 \times 10^{-6}$/K,[26] while $\alpha_{PT} = 12.6 \times 10^{-6}$/K and $\alpha_{BT} = 9.8 \times 10^{-6}$/K).[27] At the high growth temperature, PBT is cubic. As the film cools below the Curie temperature, PBT transforms to the ferroelectric tetragonal phase and experiences compressive stress on single-crystal MgO (promoting *c*-axis orientation) while PBT on biaxially textured $MgO/Si_3N_4/Si$ experiences tensile stress (promoting *a*-axis formation).

The PBT films of various compositions were deposited on MgO and the variation of lattice parameters, determined from normal θ–2θ scans, with Pb content (*x*) is consistent with the published results[28] on bulk powder as shown in Fig. 2. The Pb content was measured using electron microprobe analysis (EMPA). For thin films, the tetragonality ratio, *c*/*a,* was found to be slightly less than what is expected for the stress-free PBT powder.

B. Imaging

Surface images (Fig. 3) showed features, 200–400 nm in size, for PBT films on single crystal MgO while films deposited on biaxially textured MgO templates had smaller grain sizes, 40–90 nm. Cross-sectional SEM (Fig. 4) revealed crack-free cross-sections with uniform thicknesses as well as clean interfaces. No impurities were detected using EDS. The small PBT grain size on the biaxially textured templates is most likely due to the reduced size of the MgO grains that is characteristic of the IBAD process.

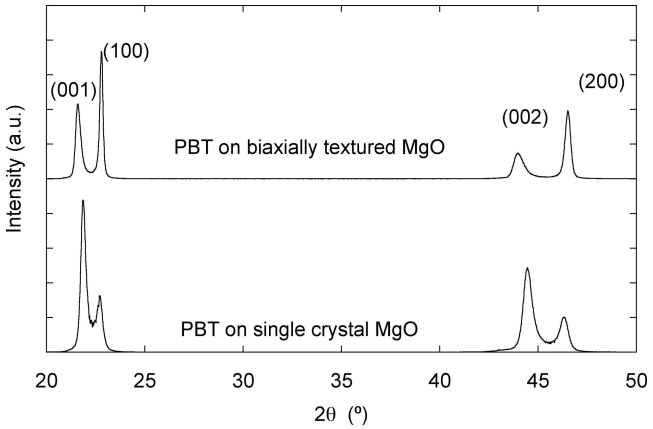

FIG. 1. XRD comparison of PBT on single-crystal and biaxially textured MgO buffer layers on Si.

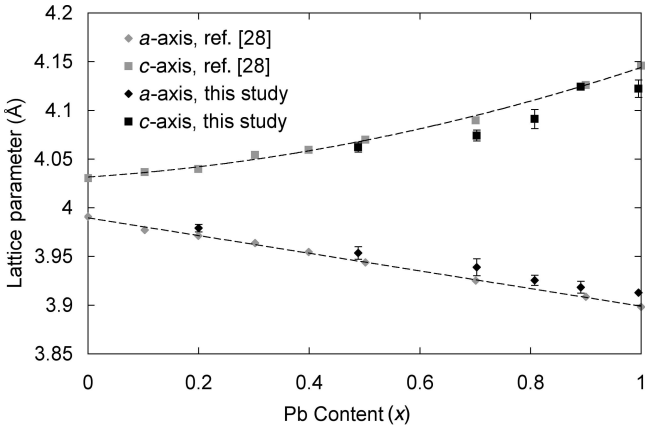

FIG. 2. Variation of PBT thin film lattice parameters with composition.

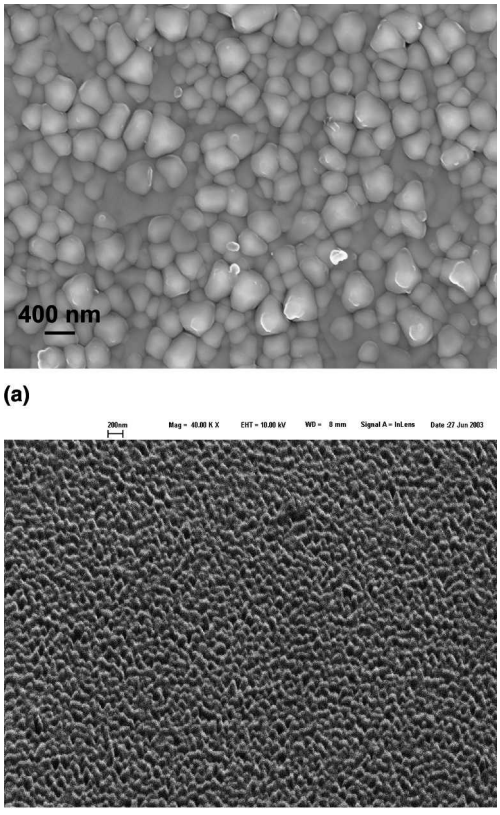

FIG. 3. Surface secondary electron images from PBT films ($x = 0.95$) on (a) single-crystal MgO and (b) biaxially textured MgO templates/Si_3N_4/Si.

C. Domain characterization

The tetragonal distortion in PBT ($c/a \neq 1$) causes a tilt angle, δ, between the (100) plane of the *a* domains and

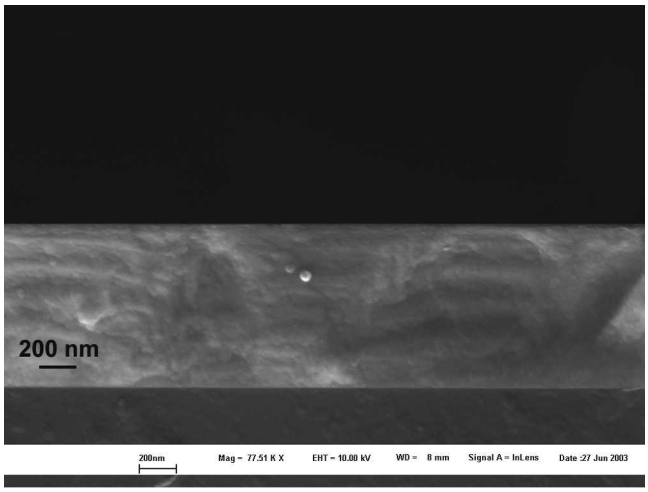

FIG. 4. Cross-sectional SEM image of PBT film on single-crystal MgO.

(001) plane of the *c* domains, as illustrated in Fig. 5. As a result, it is not possible to get a complete picture of domain orientation in PBT using normal x-ray θ–2θ scans alone. The x-ray pole figures are necessary for a comprehensive understanding of the domain orientation.[29]

For the PBT thin films examined in this study, the *c* domains were observed to be oriented normal to the sample's surface while the *a* domains were tilted, by the angle δ, in four equivalent directions away from the substrate normal, giving rise to four variants. A sample (100) pole figure (Fig. 6) for PT on single-crystal MgO, is 4-fold split, indicating the presence of these four variants. The 4-fold splitting, observed here for various compositions of PBT on single-crystal MgO, is the direct signature of 90° domain walls in the films.

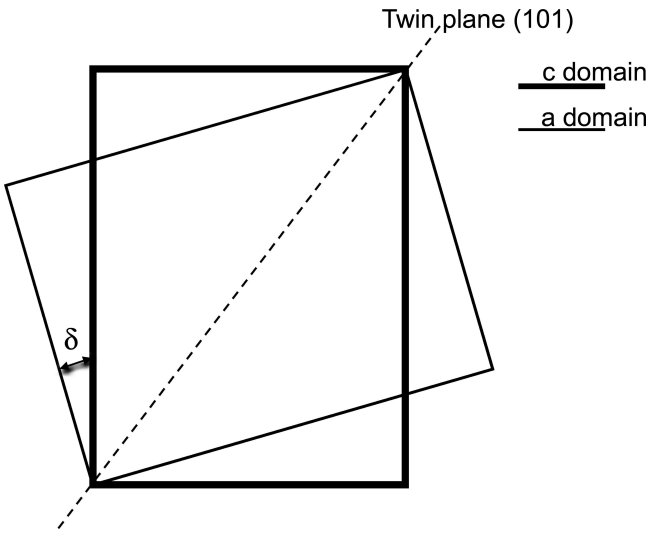

FIG. 5. Misorientation angle of *c* and *a* domains separated by (101) twin plane (exaggerated). The misorientation can lie in any of four directions (1 shown) due to the unit-cell symmetry.

In principle, the tilt of the *a* domains would lead to θ–2θ normal scans underestimating the abundance of *a* domains when calculating the domain fractions from the integrated intensities of diffraction peaks.[30] In this study, domain volume fractions for a variety of PBT compositions and film thicknesses were calculated using θ–2θ scans (using integrated intensities from the first-order diffraction peaks) and pole figures (using full volume integration of the (001) and (100) poles) at room temperature. The normal scans were found to underestimate the *a* domain volume fraction, but only slightly. For instance, direct comparison of domain fractions from pole figure volume integration and θ–2θ scans, at room temperature, differed only by 3% for a 400 nm, $x = 0.8$ PBT film and only 5% for a 250-nm PT film (composition $x = 1$, where the tilt angle is maximum). As the temperature increases, the tetragonality ratio, *c*/*a* (confirmed experimentally using the θ–2θ scans), as well as the tilt angle, δ, decrease. This further improved the domain fraction results from the θ–2θ scans. For this reason, θ–2θ scans will be used below to estimate the extent of domain switching at higher temperatures.

Pole figures, both (001) and (100), were also collected for films deposited on biaxially textured IBAD MgO substrates. These data exhibited no such pole splitting, suggesting the absence of twin boundaries (Fig. 6). The presence of 90° domain walls only for films grown on single-crystal MgO is consistent with results obtained using cross-sectional transmission electron microscopy (XTEM), on similarly prepared films.[31] In XTEM images (Figure 7) of a PBT film on single-crystal MgO, a regularly spaced domain structure is observed, where *a* domains appear as wedges oriented at about 45° to the normal in the predominantly *c*-axis film. No such structure was observed for a PBT film on the biaxially textured $MgO/Si_3N_4/Si$ template grown in the same batch, under the same processing conditions.[17]

Plan view TEM indicated that the grain size for PBT on biaxially textured MgO (60 nm average) was indeed smaller than that for PBT on single-crystal MgO. We propose that this reduced grain size is the primary reason for absence of the 90° domain walls. It has been observed that a domain-structure transition, from multi-domain to single-domain grains, occurs for small grain sizes (~150 nm),[32] resulting in whole *c*- or *a*-oriented grains. This is consistent with the absence of domain boundaries (from pole figures and XTEM) for the films on biaxially textured substrates, where the grain size is well below this limit.

D. Microtexture

Inverse pole figures (IPFs) were calculated from EBSD data, as a convenient texture representation for the thin film geometry, where single-axis textures can be

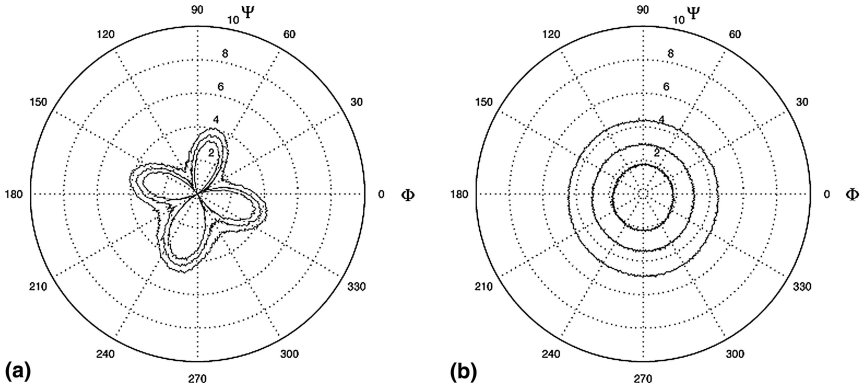

FIG. 6. Simplified (100) pole figures of PT thin films. Four-fold splitting is observed for PT on single-crystal MgO (a), indicating the presence of 90° domain walls. No twin boundaries are observed for PT on IBAD $MgO/Si_3N_4/Si$ (b).

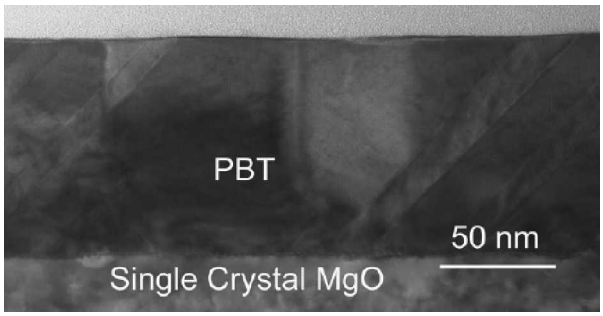

FIG. 7. XTEM image of the domain structure observed for PBT film on single-crystal MgO consistent with pole figures (from Ref. # 31).

displayed (normal to or in-plane of substrate for instance). IPFs were consistent with XRD results, indicating that the vast majority of sample patterns are either (001) or (100) oriented for PBT, on both types of substrates (Fig. 8 for 500 nm PBT films, $x = 0.9$). Furthermore, the in-plane (Y0-IPF along MgO 001 in the plane of substrate) and out-of-plane (Z0-IPF along surface normal) textures had a smaller mosaic spread for samples on single-crystal MgO compared to biaxially textured MgO templates, as is expected.

The *c* versus *a* domain fractions can also be estimated using EBSD from the normal axis IPF, by simply counting the number of data points that cluster around the 001 and 010 poles. It must be noted, however, that the penetration depth of EBSD is only 30–60 nm compared to a few micrometers using XRD. The domain fractions obtained from EBSD, therefore, will represent the near-surface domain structure except for very thin films. Domain fractions obtained using EBSD were within 5–10% of XRD data for PBT films less than 100 nm in thickness. For thicker films (~500 nm), we observed differences as large as 30%, where the EBSD data typically overestimated the abundance of the minority domain orientation.

The EBSD data were also consistent with the observation of the tetragonal tilt angle, where *a* domains (for PBT on single-crystal MgO) were tilted from the surface normal by δ (see Fig. 5). The orientation data, gathered from the *a*-oriented sample points, showed the majority of *a* domains were tilted 2–3° away from the surface normal (Fig. 9) compared to a standard distribution for the *c* domains. This spike agrees well, with the expected tilt angle value for this film, where $c/a = 1.051$ and $\delta = 2 \arctan(c/a) - 90° = 2.85°$. No such spikes were found for PBT films on biaxially textured MgO, further confirming the absence of 90° domain boundaries in these films, due to the reduced grain size.

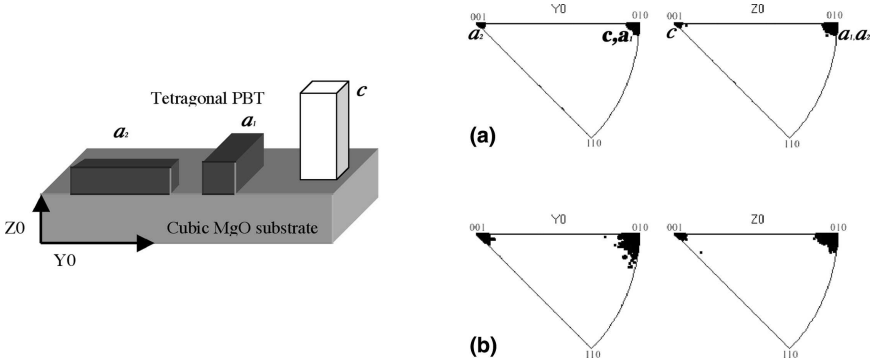

FIG. 8. Inverse pole figures for 500-nm PBT thin films ($x = 0.9$) on (a) single-crystal MgO and (b) biaxially textured IBAD MgO. The *Y*0 and *Z*0 axes are aligned with the MgO ⟨001⟩, as illustrated above. The *c* and *a* domains are illustrated and labeled on the appropriate IPF.

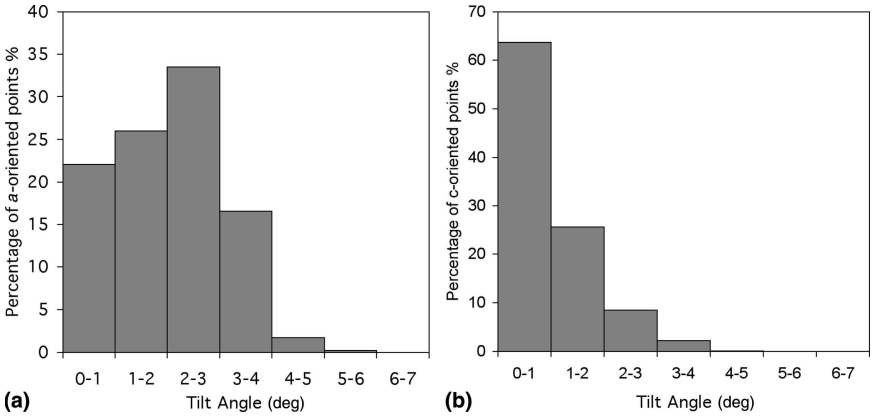

FIG. 9. EBSD confirms the tilt of *a* domains away from surface normal by the angle δ (a), while *c* domains exhibit a standard distribution (b). Results for 500-nm PBT film ($x = 0.9$) on single-crystal MgO. The tilt is consistent with x-ray pole figures and is the direct signature of ferroelectric 90° domain boundaries.

E. Domain switching

There is experimental and theoretical evidence[33–40] that the domain structure forms as a strain-accommodating mechanism, when the system cools through the Curie temperature following growth. The net effect is to minimize the total energy of the heterostructure, using the degree of freedom that the tetragonal phase offers in the form of domain switching. In terms of the coherent temperature-dependent stability map,[33] the films fabricated in this study occupy the mixed *a*/*c* portion of the map. This is predicted and experimentally observed for PT on MgO using an effective substrate lattice parameter, *b**, to take into account the misfit dislocations at the film/substrate interface formed during growth.[34,37]

High-temperature x-ray diffraction (HTXRD) scans, for PBT on single-crystal MgO, did indeed show a substantial change in *c* and *a* domain volume fractions as a function of temperature up to the phase-transition point, as evidenced by the change of intensity of (001) and (100) diffraction peaks. Figure 10 features a series of θ–2θ scans of the first order diffraction peaks from a 240-nm PT thin film on single-crystal MgO. These spectra indicate, that in addition to domain fraction changes, the *c* lattice parameter decreases with temperature while the *a* lattice parameter increases, as first observed by Shirane[41] on bulk PT. The spectra are consistent with work predicting and experimentally verifying the change of domain fractions for PT on MgO[38,39] and we here expand the range of compositions for which domain switching with temperature is verified.

A variety of compositions ($x \sim 0.5$–1) have been tested and all displayed domain changes similar to the PT/MgO system featured in Fig. 10. The volume fractions were extracted from the θ–2θ scans by fitting pseudo-Voigt profile functions (the weighted mean between a Lorentzian and a Gaussian function) to the first-order diffraction peaks (001 and 100) to extract better data and deconvolve

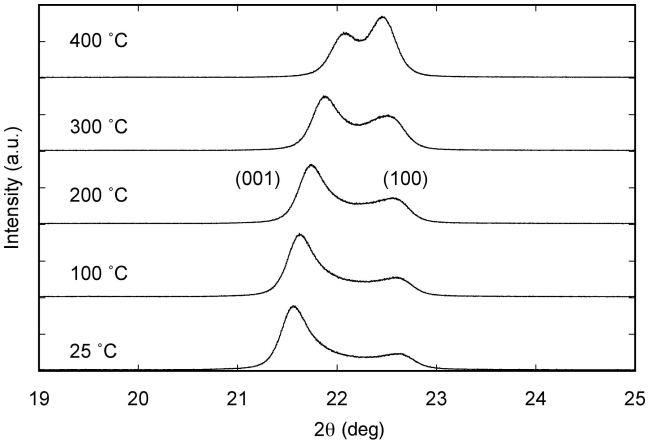

FIG. 10. Successive HTXRD scans of a 240-nm PT thin film on single-crystal MgO with increasing temperature (bottom to top). A domain transition occurs from predominantly *c*-axis-oriented film to mostly *a*-axis-oriented film at higher temperatures.

overlapping peaks. A standard nonlinear least-squares refinement procedure was used to arrive at the final fit for each temperature (Levenberg–Marquardt method). Results are shown in Fig. 11 for PT as well as a PBT film ($x = 0.7$) on single-crystal MgO. Results are not included for temperatures nearing the respective Curie temperatures, as it was difficult to reliably deconvolve the (001) and (100) peaks near the transition points.

The results presented here agree with theoretical work,[40] suggesting that for a fully relaxed PT film deposited by MOCVD under similar conditions, the *c* domain fraction is ~0.81 at room temperature (0.8 in Fig. 11). Furthermore, the reduction in the *c* domain fraction is consistent with the calculations by the same authors.

No such coherent domain switching was observed for the PT thin films deposited on IBAD $MgO/Si_3N_4/Si$. These results, coupled with the absence of 90° domain

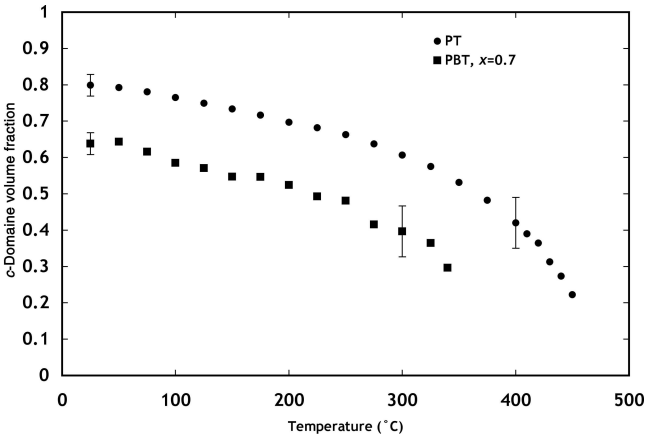

FIG. 11. Change of *c* domain fraction with temperature for a 240-nm PT thin film and a 450-nm PBT ($x = 0.7$) film on single-crystal MgO.

walls (discussed above) for this type of substrate (due to reduced grain size) suggest that 90° domain boundaries may be critical for the process of domain switching as a strain relief mechanism. Instead, the whole *c*- or *a*-oriented grains appear to be pinned to the substrate in this specific heterostructure.

IV. CONCLUSION

$Pb_xBa_{1-x}TiO_3$ ferroelectric thin films were successfully deposited on both single-crystal MgO and biaxially textured $MgO/Si_3N_4/Si$ substrates using MOCVD. A systematic comparison using SEM, XTEM, XRD, and XRD pole figures indicated the absence of 90° twin boundaries for PBT on the biaxially textured MgO and we attribute this result to the reduced grain size on this type of substrate, when compared to larger PBT grains, containing twin boundaries, on single-crystal substrates. Changes in domain fractions were observed in films containing 90° domain boundaries, at higher temperatures, using HTXRD. These results are consistent with theoretical work suggesting that the domain switching acts as a strain-relief mechanism to reduce the overall energy of the heterostructure. However, no such changes were observed for films lacking twin boundaries, on biaxially textured MgO templates.

We also utilized EBSD as a tool to study the texture of the ferroelectric thin films, by presenting texture data, in the form of in-plane and normal axis IPFs that are consistent with the XRD results. Orientation data from EBSD further confirmed the presence of 90° domain boundaries for PBT on single-crystal MgO, evidenced by measuring the tetragonal tilt angle. The combination of superior resolution and large spatial extent makes EBSD a powerful tool to probe the near-surface domain microstructure and full texture information of ferroelectric thin films and microstructures directly in the SEM.

ACKNOWLEDGMENTS

The authors thank Harry Atwater, Rhett Brewer, Mathew Dicken, and Jennifer Ruglovsky (Applied Physics, Caltech) for providing the IBAD MgO templates and Carol Garland for TEM work. This work was funded by the United States Department of Defense MURI award DAAD19-01-1-0517, administered by the Army Research Office.

REFERENCES

1. P. Krulevitch, A.P. Lee, P.B. Ramsey, J.C. Trevino, J. Hamilton, and M.A. Northrup: Thin film shape memory alloy microactuators. *J. Microelectromech. Syst.* **5**(4), 270–282 (1996).
2. G. Shirane, S. Hoshino, and K. Suzuki: Crystal structures of lead titanate and of lead–barium titanate. *J. Phys. Soc. Jpn.* **5**(6), 453–455 (1950).
3. K. Bhattacharya, A. DeSimone, K.F. Hane, R.D. James, and C.J. Palmstrom: Tents and tunnels on martensitic films. *Mater. Sci. Eng. A, Struct. Mater. Properties Microstruct. Process.* **275,** 685–689 (1999).
4. K. Bhattacharya and R.D. James: A theory of thin films of martensitic materials with applications to microactuators. *J. Mech. Phys. Solids,* **47**(3), 531–576 (1999).
5. Y.F. Chen, J.X. Chen, L. Shun, T. Yu, P. Li, N.B. Ming, and L.J. Shi: Preparation of epitaxial $PbTiO_3$ thin-films by metalorganic vapor-phase epitaxy under reduced pressure. *J. Cryst. Growth* **146**(1–4), 624–629 (1995).
6. T.W. Kim and S.S. Yom: Microstructural, electrical, and transmittance properties of $PbTiO_3$ films grown on p-InP (100) substrates at low temperature. *J. Phys. Chem. Solids* **60**(7), 935–942 (1999).
7. L. Sun, Y.F. Chen, L. He, C.Z. Ge, T. Yu, M.S. Zhang, N.B. Ming, D.S. Ding, and Y.C. Chang: Epitaxial growth of $PbTiO_3$ thin film on (110)$NdGaO_3$ substrate by metalorganic chemical vapor deposition. *Z. Phys. B, Condensed Matter* **102**(4), 479–482 (1997).
8. L. Sun, Y.F. Chen, T. Yu, N.B. Ming, D.S. Ding, and Z.H. Lu: (001) Textured $PbTiO_3$ thin films grown on redoping n-Si by metalorganic chemical vapor deposition under reduced pressure. *Appl. Phys. A, Mater. Sci. Processing* **63**(4), 381–384 (1996).
9. Y.S. Yoon, S.S. Yom, T.W. Kim, D.U. Lee, and C.O. Kim: Improvement of the crystallinity in $PbTiO_3$ films grown on indium tin oxide-coated glass by metalorganic chemical vapor deposition using the continuous cooling process. *Appl. Surf. Sci.* **93**(4), 285–289 (1996).
10. T. Yu, Y.F. Chen, L. Shun, J.X. Chen, and N.B. Ming: Phase-transition of $PbTiO_3$ polycrystalline thin-film prepared by metal-organic chemical vapor deposition on yttrium-stabilized zirconium. *Solid State Commun.* **96**(7), 477–480 (1995).
11. Y. Gao, G. Bai, K.L. Merkle, H.L.M. Chang, and D.J. Lam: Effects of substrate orientation and cooling rate on microstructure of $PbTiO_3$ thin-films grown by metal–organic chemical vapor deposition. *Thin Solid Films* **235**(1–2), 86–95 (1993).
12. M. Okada, S. Takai, M. Amemiya, and K. Tominaga: Preparation of *c*-axis-oriented $PbTiO_3$ thin-films by MOCVD under reduced pressure. *Jpn. J. Appl. Phys. Part 1, Reg. Papers Short Notes Rev. Papers* **28**(6), 1030–1034 (1989).
13. M. Dekeijser, D.M. Deleeuw, P.J. Vanveldhoven, A.E.M. Deveirman, D.G. Neerinck, and G.J.M. Dormans: The structure of heteroepitaxial lead titanate layers grown by organometallic chemical vapor deposition. *Thin Solid Films* **266**(2), 157–167 (1995).
14. H. Nakazawa, H. Yamane, and T. Hirai: Metalorganic chemical vapor deposition of $BaTiO_3$ films on MgO(100), *Jpn. J. Appl.*

Phys. Part 1, Regular Papers Short Notes Rev. Papers **30**(9B), 2200–2203 (1991).
15. J.M. Zhang, C.P. Beetz, and S.B. Krupanidhi: Photoenhanced chemical vapor deposition of $BaTiO_3$. *Appl. Phys. Lett.* **65**(19), 2410–2412 (1994).
16. P. Schafer, S. Ritter, R. Ganster, P. Ehrhart, S. Hoffmann, and R. Waser: Preparation of $(Pb_xBa_{1-x})TiO_3$ thin films by MOCVD using an aerosol-assisted liquid delivery system. *Integrated Ferroelectrics* **30**(1–4), 165–173 (2000).
17. R.T. Brewer, D.A. Boyd, M.Y. El-Naggar, S.W. Boland, Y.B. Park, S.M. Haile, D.G. Goodwin, and H.A. Atwater: Growth of biaxially textured $Ba_xPb_{1-x}TiO_3$ ferroelectric thin films on amorphous Si_3N_4. *J. Appl. Phys.* **97**(3), 2005 (Art. No. 034103).
18. C.P. Wang, K.B. Do, M.R. Beasley, T.H. Geballe, and R.H. Hammond: Deposition of in-plane textured MgO on amorphous Si_3N_4 substrates by ion-beam-assisted deposition and comparisons with ion-beam-assisted deposited yttria-stabilized-zirconia. *Appl. Phys. Lett.* **71**(20), 2955–2957 (1997).
19. D. Chateigner, H.R. Wenk, A. Patel, M. Todd, and D.J. Barber: Analysis of preferred orientations in PST and PZT thin films on various substrates. *Integrated Ferroelectrics* **19**(1–4), 121–140 (1998).
20. C.J. Kim, D.S. Yoon, J.S. Lee, C.G. Choi, W.J. Lee, and K. No: Electrical characteristics of (100), (111), and randomly aligned lead–zirconate–titanate thin films. *J. Appl. Phys.* **76**(11), 7478–7482 (1994).
21. S. Mansour and R. Vest: The dependence of ferroelectric and fatigue behaviors of PZT films on microstructure and orientation. *Integrated Ferroelectrics* **1,** 57–69 (1992).
22. A. Tripathi: In situ diagnostics for metalorganic chemical vapor deposition of YBCO. Ph.D. Thesis, California Institute of Technology, Pasadena, CA, 2001.
23. W.J. Desisto and B.J. Rappoli: Ultraviolet absorption sensors for precursor delivery rate control for metalorganic chemical vapor deposition of multiple component oxide thin films. *J. Crystal Growth* **191**(1–2), 290–293 (1998).
24. *Electron Backscatter Diffraction in Materials Science,* edited by A.J. Schwartz, M. Kumar, and B.L. Adams (Kluwer Academic, New York, 2000).
25. *Properties of Crystalline Silicon,* edited by R. Hull (Institute of Electrical Engineers, London, U.K., 1999).
26. *Thermal Expansion of Nonmetallic Solids,* Vol. 13 of Thermophysical Properties of Matter, edited by Y. Touloukian, R. Kirby, R. Taylor, and T. Lee (IFI/Plenum, New York, 1977).
27. *Piezoelectric Ceramics,* Vol. 3 of Non-metallic Solids, edited by B. Jaffe, W.R. Cook, and H.L. Jaffe (Academic Press, New York, 1971).
28. G. Burns: Lattice modes in ferroelectric perovskites 2. $Pb_{1-x}Ba_xTiO_3$ including $BaTiO_3$. *Phys. Rev. B* **10**(5), 1951–1959 (1974).
29. A. De Veirman, J. Cillessen, M. De Keijser, R. Wolf, D. Taylor, A. Staals, and G.J.M. Dormans: In *Epitaxial Oxide Thin Films and Heterostructures,* edited by D.K. Fork, J.M. Phillips, R. Ramesh, and R.M. Wolf (Mater. Res. Soc. Symp. Proc. **341,** Pittsburgh, PA, 1994), pp. 329–340.
30. W.Y. Hsu and R. Raj: X-ray characterization of the domain-structure of epitaxial lead titanate thin-films on (001)-strontium-titanate. *Appl. Phys. Lett.* **67**(6), 792–794 (1995).
31. R. Brewer: Quantitative Biaxial Texture Analysis with Reflection High-Energy Electron Diffraction for Ion Beam-Assisted Deposition of MgO and Heteroepitaxy of Perovskite Ferroelectrics; Ph.D. Thesis; California Institute of Technology, Pasadena, 2004.
32. S.B. Ren, C.J. Lu, J.S. Liu, H.M. Shen, and Y.N. Wang: Size-related ferroelectric-domain-structure transition in a polycrystalline $PbTiO_3$ thin film. *Phys. Rev. B* **54**(20), 14337–14340 (1996).
33. J. Speck and W. Pompe: Domain configurations due to multiple misfit relaxation mechanisms in epitaxial ferroelectric thin films. I. Theory. *J. Appl. Phys.* **76**(1), 466–476 (1994).
34. J. Speck, A. Seifert, and W. Pompe: Domain configurations due to multiple misfit relaxation mechanisms in epitaxial ferroelectric thin films. II. Experimental verification and implications. *J. Appl. Phys.* **76**(1), 477–483 (1994).
35. B.S. Kwak, A. Erbil, J.D. Budai, M.F. Chisholm, L.A. Boatner, and B.J. Wilkens: Domain formation and strain relaxation in epitaxial ferroelectric heterostructures. *Phys. Rev. B* **49**(21), 14865–14879 (1994).
36. J. Speck, A. Daykin, and A. Seifert: Domain configurations due to multiple misfit relaxation mechanisms in epitaxial ferroelectric thin films. III. Interfacial defects and domain misorientations. *J. Appl. Phys.* **78**(3), 1696–1706 (1995).
37. C. Foster, W. Pompe, A. Daykin, and J. Speck: Relative coherency strain and phase transformation history in epitaxial ferroelectric thin films. *J. Appl. Phys.* **79**(3), 1405–1415 (1996).
38. N. Pertsev and A. Zembilgotov: Energetics and geometry of 90-degree domain structures in epitaxial ferroelectric and ferroelastic films. *J. Appl. Phys.* **78**(10), 6170–6180 (1995).
39. N. Pertsev and A. Zembilgotov: Domain populations in epitaxial ferroelectric thin films: Theoretical calculations and comparison with experiment. *J. Appl. Phys.* **80**(11), 6401–6406 (1996).
40. S.P. Alpay and A.L. Roytburd: Thermodynamics of polydomain heterostructures. III. Domain stability map. *J. Appl. Phys.* **83**(9), 4714–4723 (1998).
41. G. Shirane, S. Hoshino, and K. Suzuki: X-ray study of the phase transition in lead titanate. *Phys. Rev.* **80**(6), 1105–1106 (1950).